mater.scichina.com link.springer.com

Published online 1 April 2022 | https://doi.org/10.1007/s40843-021-2004-6
Sci China Mater 2022, 65(8): 2262–2273

SPECIAL ISSUE: Flexible Intelligent Materials

Bioinspired wet-resistant organogel for highly sensitive mechanical perception

Wen Zhao[1,4], Dingli Gan[1], Xinyu Qu[1], Jingying Liu[1], Yunlong Liu[2], Qian Wang[1*], Wenjun Wang[2], Chencheng Sun[3*] and Xiaochen Dong[1*]

ABSTRACT **Smart flexible electronics with underwater motion detection have become a promising research aspect in intelligent perception. Inspired by the strong adaptability of marine creatures to complex underwater environments, conventional biocompatible hydrogels are worth developing into organogels with preferred underwater adhesive properties, hydrophobic and antiswelling performance, and motion perception ability. Herein, a highly sensitive organogel sensor exhibiting good hydrophobicity, electromechanical properties, and adhesion properties was prepared for underwater utilization by regulating the chemical components and internal interactions. The synergistic effect of massive reversible noncovalent bonds ensures the organogel's excellent underwater adhesion to multifarious substrates. Meanwhile, the interactions of hydrophobic conductive fillers and the dynamic hydrophobic associations in the organogel endow it with satisfactory hydrophobic performance (contact angle of 111.8°) and antiswelling property (equilibrium swelling ratio of −31% after 15-day immersion). The fabricated flexible organogel strain sensor exhibits high sensitivity (gauge factor of 1.96), ultrafast response rate (79.1 ms), low limit of detection (0.45 Pa), and excellent cyclic stability (1044 tensile cycles followed by 3981 compressive cycles). Results demonstrate the proposed organogel's precise perception of sophisticated human motions in air and underwater, which expands its application scenarios.**

Keywords: flexible electronics, organogel, hydrophobic association, water-resistant, underwater application

INTRODUCTION

Hydrogels, which exhibit skin-like softness, high ductility, and biocompatibility, are desirable in various scenarios of drug delivery [1], human physiology monitoring [2], human-machine interaction [3], and wound dressings [4]. Particularly, the flourishing of flexible wearable devices provides new opportunities for hydrogel development [5–8]. By rational material screening and structure design, hydrogel sensors can achieve satisfactory mechanical and electrical performance to meet the requirements of wearable flexible electronics [9–12]. However, when utilized in a humid environment or underwater, hydrogel sensors are severely prone to swelling-incurred structural collapse.

The dynamic hydrophobic association inside the gel and its hydrophobic surface could inhibit the penetration of water molecules into the polymer matrix and protect it against massive intermolecular interactions to retain the mechanical strength and electrical sensing properties of the gel in an aqueous environment [13,14]. The hydrophobic interface plays a critical role in the formation of a water-resistant molecular bridge between the gel and the substrate, which further repels surrounding water molecules [15]. Grafting hydrophobic groups onto polymer skeletons is one widely employed strategy to promote hydrophobicity. However, the complicated preparation processes and byproducts inevitably damage gel performances and thus limit their applications. Therefore, the copolymerization of hydrophilic monomers and hydrophobic branches is proposed to realize reliable perception with long-term stability underwater.

In addition, the interfacial hydration overlayer reduces the conformability of hydrogels to achieve high-precision perception by inhibiting the formation of molecular bridges to weaken the noncovalent interaction between the adhesive and the substrate [16] or inducing swelling stress to deteriorate interfacial adhesion [17]. Marine animals have achieved interfacial adhesion in a humid environment through hyperfine microstructures [18]. For example, mussels can firmly cling to the rough and humid seabed through Mfps, a protein with catechol groups that can form noncovalent interactions (e.g., π–π stacking or hydrophobic bonding) with various surfaces and possess strong adhesion ability [19,20]. Inspired by this natural phenomenon, some catechol-modified gels have been promoted for flexible underwater electronics. Ji *et al.* [21] prepared a stretchable and highly adhesive electrode to realize real-time underwater electrocardiography. The polydopamine-modified surface enables the close attachment of the electrode to the skin with high conformability. However, the highly chemically activated O-

[1] Key Laboratory of Flexible Electronics (KLOFE) & Institute of Advanced Materials (IAM), School of Physical and Mathematical Sciences, Nanjing Tech University (NanjingTech), Nanjing 211816, China
[2] School of Physical Science and Information Technology, Liaocheng University, Liaocheng 252059, China
[3] School of Electronic and Information Engineering, Changshu Institute of Technology, Changshu 215500, China
[4] Department of Mechanical Engineering, City University of Hong Kong, Hong Kong 999077, China
[*] Corresponding authors (emails: iamxcdong@njtech.edu.cn (Dong X); chelseawq@njtech.edu.cn (Wang Q); ccsun@cslg.edu.cn (Sun C))

hydroxyphenyl is easily oxidized to form poor stickiness quinone, which severely depresses the adhesion property of the gel [22]. Moreover, the obtained oxides quench free radicals, seriously hinder polymerization, and reduce polymer performance [23]. A delicate design of polymer matrices and interactions could effectively protect catechol groups from oxidation [24,25]. For example, Cui's group [26] presented metal ion incorporation after conventional polymerization reaction to implement the reversible underwater adhesion of the targeted gel. Specifically, Fe^{3+} displayed enhanced interaction with catechol to induce surface rearrangement and promote reversible metal coordination, thereby playing a critical effect on achieving nonspecific underwater adhesion. Furthermore, nanomaterials, such as silver nanoparticles (Ag NPs) and silver nanowires (Ag NWs), could reduce the oxygen content in the system to inhibit catechol oxidation with spatial confinement effects [27]. Gan *et al.* [28] prepared a strong adhesive gel based on Ag NPs and constructed a redox system to produce sustained catechol groups. The highly conductive and hydrophobic Ag NWs also endowed the gel with excellent electromechanical performance, serving as an ideal candidate for hydrogel conductive fillers. The synergistic effects of noncovalent bonds and nanofillers offer a universal approach to endow gels with stable and reproducible underwater adhesion ability and intelligent mechanical perception. Therefore, self-adhesive conductive organogels capable of adapting to humid environments should urgently be developed.

Herein, a hydrophobic organogel sensor that could realize contactless information detection through Morse code, remote recognition of aqueous environment changes, and even identification of different gestures was fabricated. The two-step preparation process, including the *in situ* free-radical copolymerization of hydrophilic and hydrophobic monomers and the subsequent Fe^{3+}-induced surface rearrangement, was proposed to endow the organogel with excellent underwater adhesion and sensing performance. Through various covalent and noncovalent interactions, the fabricated organogel could rapidly, firmly, and repeatedly stick to various substrates in air and underwater while exhibiting excellent antiswelling properties. The organogel sensor could be assembled to monitor underwater human motion. Meanwhile, its high sensitivity to water vibration facilitates the contactless perception of motions, and it thus shows great promise in remote underwater communication.

EXPERIMENTAL SECTION

Materials

N-isopropyl acrylamide (NIPAM, >98%), octadecyl acrylate (OA, >98%), *N*,*N*′-methylene bisacrylamide (MBAA, >99%), and 2,2′-azobisisobutyronitrile (AIBN, >98%) were purchased from Adamas Reagent Co., Ltd. Catechol (CT, >98%), sodium dodecyl sulfate (SDS, >86%), iron(Ⅲ) chloride hexahydrate ($FeCl_3{\cdot}6H_2O$, >99%), and dimethyl sulfoxide (DMSO, >99%) were supplied by Sinopharm Chemical Reagent Co., Ltd. The Ag NWs (10 mg mL^{-1}) were obtained from C3nano.

Preparation and characterization of organogels

The organogel, abbreviated as SACON-F, was prepared through the *in situ* free-radical polymerizations of hybrid hydrophilic and oleophilic monomers, followed by a solvent exchange process. First, 0.80 g of NIPAM, 0.20 g of OA, 0.28 g of SDS, and 2 mg of catechol were dissolved in 4 mL of DMSO at 25 ± 5°C with ultrasound dispersion. Then, 50 mg of the Ag NW solution, 27 mg of the crosslinking agent MBAA, and 10 mg of the initiator AIBN were added into the mixed solution under vigorous stirring. After dispersion, the solution was poured into a mold and transferred to an oven. After polymerization at 70°C for 8 h, a prepolymer gel was formed and denoted as SACON. Finally, the prepolymer SACON was immersed in 20 mL of $FeCl_3$/DMSO solution (0.12 mol L^{-1}) for 80 min for solvent exchange. The organogel SACON-F was then obtained. Different organogels were prepared herein to comprehensively study the influence of the gel compositions and additive contents on the gel properties, and detailed descriptions of the compositions of each organogel are described in Table S1. Specifically, ON denotes the organogel containing OA and NIPAM, AON denotes the organogel of OA, NIPAM, and AgNWs. The pre-organogels with the $FeCl_3$/DMSO solution (0.12 mol L^{-1}) immersion were labeled as "prepolymer-F."

The electrical conductivity of SACON-F was tested by performing linear scanning voltammetry on an electrochemical analyzer (CHI660D, Chenhua). The sample was tailored into a strip of 30 mm × 5 mm × 2 mm, and the conductivity σ was calculated on the basis of the following formula: $\sigma = l/(R \times S)$, where R is the resistance of the gel, S is the cross-sectional area of the sample, and l is the length of the sample.

Water contact angle measurement

In characterizing the wettability of the gel surface, 2 μL of water droplets was quickly dropped on the surface of a 30 mm × 30 mm PNIPAM hydrogel or SACON-F at 25 ± 2°C, and an optical contact angle meter (DSA series) was utilized to record the water contact angle in real time. In addition, the surface contact angle was characterized after applying a 100% strain to the SACON-F to elaborate the evolution of hydrophilic property under tensile conditions.

Antiswelling and dehydration characterization

The antiswelling ratio of the organogels was measured as follows: cylindrical samples were prepared with a diameter of 10 mm and a thickness of 2 mm. Then, the samples were soaked in 5 mL of deionized water for 15 days at 0, 25, and 50°C. The weight of each sample was measured every 2 h for the first three days and every 12 h in the succeeding days. Each experiment was repeated three times to obtain a mean value. The swelling rate (SR) can be calculated as follows:

$$\mathrm{SR}(\%) = \frac{W_s - W_0}{W_0} \times 100\%, \quad (1)$$

where W_0 is the weight of the organogels before the swelling tests and W_s is the weight of the organogels after immersion.

A piece of the cylindrical sample (Φ 10 mm × 2 mm) was also prepared to test the moisture retention abilities of the organogels. The specific gel was placed at 0, 25, and 50°C with 50% ± 10% relative humidity (RH) for 15 days and weighed every 2 h in the first three days and every 12 h thereafter. The experiment was repeated three times to obtain an average value. The solvent retention capability of the gels was estimated from the dehydration rate (Q), which can be calculated from Equation (2):

$$Q(\%) = \frac{W_0 - W_t}{W_0} \times 100\%, \quad (2)$$

where W_0 is the pristine weight of the organogel and W_t is the

weight of the organogel after dehydration.

Adhesive and mechanical performance measurement

A peeling test was conducted to evaluate the shear adhesion property of the gel. A strip of 20 mm × 20 mm × 2 mm was clamped between two pieces of metal, glass, polypropylene (PP), or polyethylene (PE) films. Then, the two pieces of materials were stretched in the opposite direction parallel to the interface at 10 mm min^{-1} until stripping. The adhesive strength was calculated by the average maximum tensile force divided by the adhesive area. The underwater adhesion test included a pressing process and a stretching process: the organogel was pressed against the substrate at certain pressures (5–50 kPa) for 1–20 min, and the pulling-off tests were conducted underwater. The mechanical performance of SACON-F-10, SACON-F-15, SACON-F-20, and SACON-F-25 was then measured under a preloading pressure of 25 kPa and a tableting time of 10 min to characterize the influence of C_{18} content on the adhesion property of the gel. All experiments were repeated three times, and the average value was taken with the standard deviation.

The mechanical properties of the organogel were measured using a tensile machine (ESM301, Mark-10) and a dynamometer (M 4-2). For the tensile fracture test, the organogel was cut into a strip of 30 mm × 5 mm × 2 mm, which was clamped between two ends in the stretching machine (with an initial length of 5 mm) and stretched at a speed of 60 mm min^{-1} in the air or an aqueous solution until the sample ruptured. The tensile strength and fracture strain were recorded in real time. For the mechanical stability in an aqueous solution, the gels were cyclically stretched between 0% and 268% strain (2 mm × 5 mm × 2 mm) or compressed from 0% to 60% deformation (Φ 25 mm × 50 mm), respectively.

Electrical performance characterization

The electrical responsiveness of SACON-F under various deformations was obtained by a semiconductor characterization system (Keithley 4200-SCS). SACON-F was cut into strips (30 mm × 5 mm × 2 mm) or cylindrical specimens (Φ 25 mm × 50 mm) and fixed on the tensile platform with wires drawn at both ends. A 1-V bias voltage was applied to the two ends of the gel strain sensor, and the current/resistance variations of the gel during tension/compression were obtained. For electrical response sensitivity detection, the gauge factor (GF) was presented and calculated using Equation (3):

$$\mathrm{GF}=\frac{\Delta R/R_0}{\varepsilon}\times 100\%, \tag{3}$$

where $\Delta R = R - R_0$, ε is the strain applied to the sensor, R_0 is the resistance of the pristine sensor, and R is the resistance of sensors after the stretching process. The gel was stretched or compressed at a speed of 10 mm min^{-1}, and the current response of the sensor under different tension or compression deformations or at different frequencies was obtained. For the response time, a 7.5% tensile strain or 48 Pa pressure was applied to the sensor at a speed of 330 mm min^{-1}, and the response current of the sensor was recorded in real time. Furthermore, 75% tensile strain or a pressure of 8.46 kPa was applied repeatedly to a special-shaped specimen to profile the electrical cycle stability. The strength of the gel was simultaneously measured to test its hysteresis. For human motion detection, the sensor adhered to different joint sites, and the real-time current signals under activities were obtained.

RESULTS AND DISCUSSION

Preparation of SACON-F

Tough adhesion to moist surfaces is a fascinating property of marine animals. For instance, mussels can reversibly adhere to various surfaces, and pufferfish can repeatedly transfer between hydrophilic and hydrophobic states by inflating themselves, thus achieving excellent adhesion in a complicated aquatic environment [18]. Typically, the polymeric structure of adhesive hydrogel plays a critical role in long-term and excellent adhesion in a highly moist environment. Herein, hydrophobic monomer OA and hydrophilic monomer NIPAM were copolymerized to construct an amphipathic organogel with antiswelling and underwater adhesion properties. The preparation process is schematically profiled in Fig. 1a. NIPAM and OA monomers were first *in situ* polymerized at 70°C to form a sequential block copolymer, and the covalent bonds between NIPAM and OA formed the first polymer network. During the subsequent immersion in $FeCl_3$/DMSO solution, the solvent exchange acti-

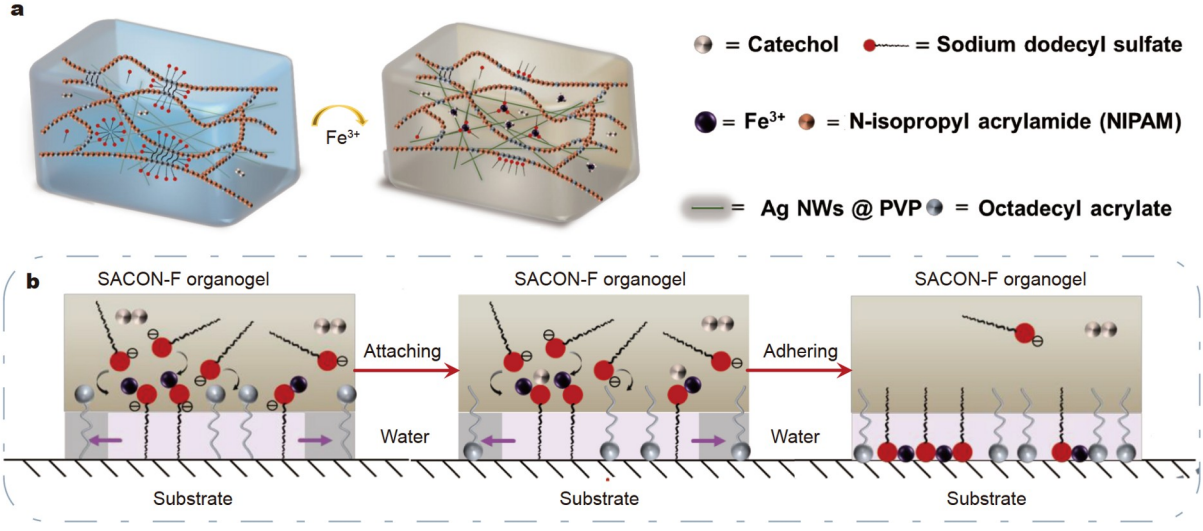

Figure 1 Schematic of preparation and internal interactions of SACON-F.

vated the aggregation of hydrophobic monomers and enhanced the cohesion of organogels, thereby providing a compact network structure for water-resistant properties. Meanwhile, the self-adjustment on surficial functional groups was beneficial to establishing a water-resistant molecular bridge between the organogel surface and the hydrophobic domains on the substrates. Moreover, the multiple hydrophobic interactions could further repel water molecules away from the interface to achieve underwater adhesion (Fig. 1b). The Fourier transformed infrared spectroscopy (FTIR) spectra of SAON, SACON, and SACON-F demonstrated distinguishable peak shifts in hydroxyl group stretching and vibration absorption peaks, thus suggesting the coordination between catechol and Fe^{3+} ions (Fig. S1). The electrostatic interaction between Fe^{3+} and the negatively charged SDS cooperatively endowed the organogel with high mechanical strength by efficiently dissipating energy under deformation. Moreover, numerous reversible noncovalent interactions, including hydrogen bonds, dynamic hydrophobic associations, and π–π stacking effect, enabled strong cohesion and good adhesion [22]. Simultaneously, uniformly dispersed Ag NWs, with an aspect ratio of 2000 (Fig. S2), facilitated the formation of a continuous conduction path and promoted the charge transfer in the organogel. The conductivities of ON, AON, SACON, and SACON-F were compared, and the results are shown in Fig. S3. Relative to ON (9.78×10^{-4} S m^{-1}), SACON-F showed an electrical conductivity of 3.14×10^{-3} S m^{-1}, which is in line with that in the literature [29,30]. The addition of 0.1% Ag NWs could significantly improve the conductivity of the gel by an order of magnitude (Table S2), thereby showing great promise in highly sensitive electromechanical perceptions. SACON-F also displayed excellent flexibility and tough resistance to various mechanical deformations (Fig. S4). It could be reversibly stretched to more than 10 times its original length, and it resisted harsh cutting and heavy pressing several times without structural failure. In addition, a strip of SACON-F (30 mm × 10 mm × 0.5 mm) could directly lift a bottle containing 1 L of water without showing rupture for minutes, thereby displaying great toughness.

Water contact angle measurement

The dynamic hydrophobic association between the Fe^{3+}-induced SDS micelles and the hydrophobic monomer OA contributed to the formation of the hydrophobic organogel, which showed high resistance to water penetration. Fig. 2 compares the surface wettability of PNIPAM hydrogel and SACON-F and their evolution over time. As depicted in Fig. 2a, b, SACON-F demonstrated a hydrophobic surface with a contact angle of 111.8°, whereas the NIPAM hydrogel revealed a representative hydrophilic surface with a contact angle of 51.7°. After 10 min of static standing, SACON-F retained its properties at a contact angle of 58.7°, thus showing long-term water resistance to inhibit the infiltration of water. Specifically, SACON-F maintained its hydrophobic property stably under mechanical deformation. As shown in Fig. 2c, SACON-F was stretched to 100% strain and manifested an even higher contact angle of 124.4°. The hydrophobic functional groups were found to be exposed to the outmost surface of the organogel under stretching, thus enhancing hydrophobicity [15]. The electrostatic interaction between Fe^{3+} and SDS also made the gel cohesive and enhanced its interface hydrophobicity. Fig. 2d demonstrates that the fabricated gel could remain hydrophobic after being placed in water for 15 days with a nearly constant contact angle (119.0°). The long-term stability of its hydrophobicity demonstrates its potential application to antifouling and waterproofing activities [31].

Antiswelling and antidehydration properties

Owing to their high water content and reversible weak physical bonds, most gels would inevitably inflate or even decompose underwater. The interface contact angle of SACON-F in Fig. 2 indicates its stable hydrophobicity and consequent resistance to water penetration. The antiswelling property is also crucial for the application of gel-based sensors in a high humidity environment. The swelling-resistant property of the prepared organogels was evaluated through sustained immersion in deionized

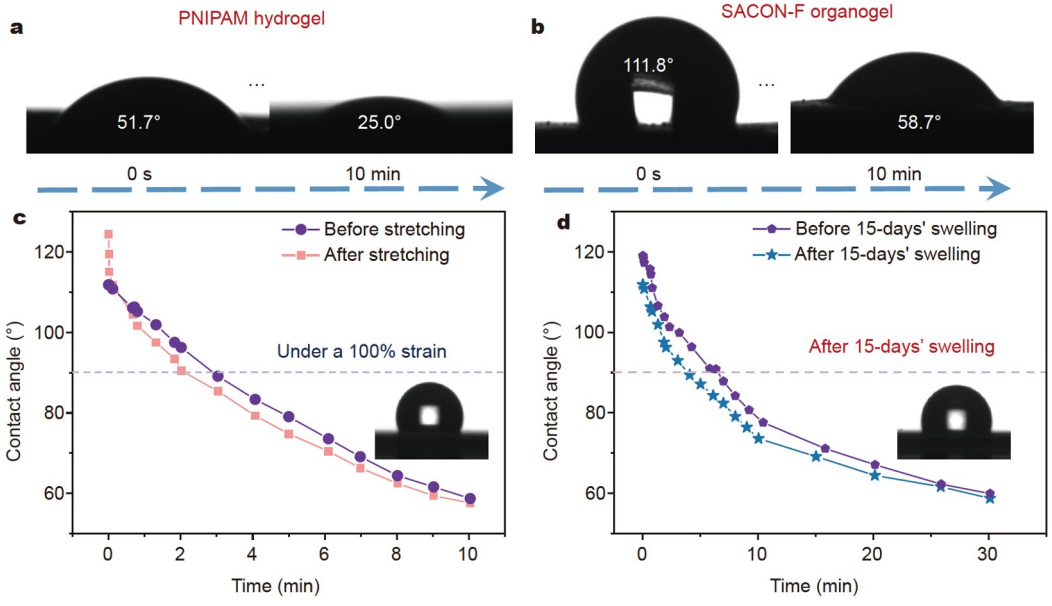

Figure 2 Contact angle analysis of the surfaces of PNIPAM hydrogel and SACON-F organogel. (a, b) Snapshots recording changes in water contact angle within 10 min on the surfaces of PINIPAM hydrogel and SACON-F. (c) Contact angle changes of SACON-F gel before and after 100% stretching. (d) Contact angle changes of SACON-F before and after swelling for 15 days.

water for 15 days. The gels presented swelling equilibrium after a certain period of immersion. Fig. 3a demonstrates the swelling evolution of PNIPAM-F, AON-F, and SACON-F at 50°C. The PNIPAM-F gel manifested a sharp increase in volume after immersion mainly because of the high hydrophilicity of the amide group. It swelled in merely 48 h with SR of 151% and reached an equilibrium swelling ratio (E_{sr}) of 184%. For AON-F gel, the swelling was greatly suppressed with E_{sr} of 51% because of the abundant hydrophobic groups on the copolymer of NIPAM and OA that supported the resistance to water penetration. By contrast, E_{sr} of SACON-F further declined to a negative value of −31% after 15 days, thus suggesting the effective inhibition of water penetration from the accessional dynamic hydrophobic association between the SDS micelles and OA. As a result of the proverbial phase change of PNIPAM at a lower critical solution temperature [32], SACON-F squeezed out the internal solvent at 50°C and showed apparent antiswelling performance. Fig. 3b compares the swelling performance of SACON-F at different temperatures. The organogels all reached swelling equilibrium within certain days, and E_{sr} increased with decreasing temperature as expected (−38% at 50°C, 148% at 25°C, and 168% at 0°C); hence, this material shows a wide prospect for high-temperature applications. Fig. S5a–c profile SACON-F after 15 days of infiltration in a series of temperatures. SACON-F maintained its original shape, thus revealing superior antiswelling performance. The strain-stress curves of SACON-F in Fig. S6a also indicate the high stability of its mechanical toughness and flexibility after being placed in water for 15 days, showing limited depression in terms of stress (29%) and stretchability (20%).

The solvent retention properties of the organogels were compared at 25°C and 50% ± 10% RH (Fig. 3c, d) to evaluate their long-term stability. During the 15 days of storage, the organogels experienced a rapid loss of solvent in the initial stage and gradually reached a stable threshold thereafter. Comparatively, after being stored for 48 h, the PNIPAM-F gel displayed the most serious dehydration, leading to shrinkage and hardening (Q = 19%), whereas AON-F and SACON-F remained elastic and lost a small amount of solvent (Q = 11% for AON-F, Q = 7% for SACON-F). The covalent bond and hydrophobic association between body OA and micellar SDS were speculated to have effectively hindered solvent diffusion and significantly slowed down solvent evaporation. Fig. 3d shows the solvent retention capability of SACON-F at different temperatures. The solvent evaporation was quite severe at 50°C with more violent molecular thermal motions, showing a nonnegligible dehydration rate of 31% after 15 days. At lower temperatures, the dehydration rate declined to 7% at 25°C and 11% at 0°C and was thus not worthy of special focus. Nevertheless, these samples maintained their dimensions despite solvent loss (Fig. S5d–f) and displayed acceptable mechanical performance attenuation after being stored at 50°C for 15 days (Fig. S6b). SACON-F demonstrated excellent antiswelling and antidehydration capabilities in a wide temperature range and appeared to be a promising candidate for flexible electronics in aquatic environments.

Underwater adhesion performance

To realize underwater force monitoring, the gel sensor should be able to adhere closely to various slippery or rough surfaces

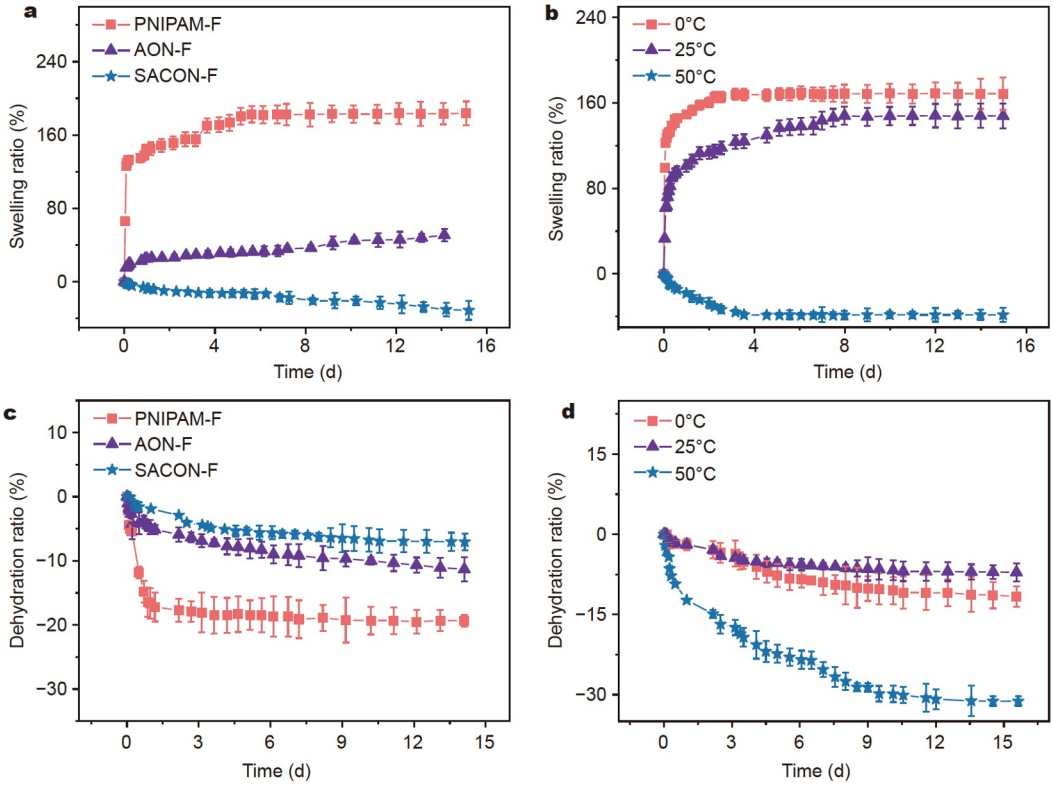

Figure 3 Environment resistance of organogels. (a) SRs of PNIPAM-F, AON-F, and SACON-F underwater. (b) Swelling ratio of SACON-F in water over time at 0, 25, and 50°C. (c) Dehydration rate of PNIPAM-F, AON-F, and SACON-F at 25°C over time. (d) Dehydration ratio of SACON-F over time at 0, 25, and 50°C.

underwater. The underlying mechanism for the expectable underwater adhesion property of SACON-F is profiled in Fig. 1b. During a typical adhesive procedure, the organogel is first compressed, and the water molecules at the organogel-adhesive interface are continuously repelled due to the OA (C_{18})-stabilized hydrophobic interface. Afterward, the organogel self-adjusts its surficial groups to achieve nonspecific interactions with different hydrophobic or hydrophilic surfaces through hydrogen bonds, hydrophobic interaction, π–π stacking, metal coordination, or electrostatic interactions [33].

The initial hydrophobic elimination of interface water stimulates the adsorptive functional groups to work, thereby exerting a critical effect on underwater adhesion. The impacts of preloaded compression strength and compression time on adhesion performance were comprehensively evaluated herein. The results showed that the adhesive strength gradually increased with the rising pressure (Fig. 4a) and reached the maximum value with 10 min tableting at 25 kPa (Fig. 4b). During the compression process, the water molecules at the organogel-adhesive interface were continuously repelled, and the size of the contact area increased. However, with an excessive preloading time, the internal hydrophilic functional groups inevitably migrated to the interface and reduced the adhesion performance. Therefore, the subsequent adhesion tests were all pre-compressed with a pressure of 25 kPa for 10 min to reach a modified performance. The hydrophobic interface was mainly attributed to the surfactants SDS and OA (C_{18}).

As illustrated in Fig. 4c, the adhesion strength of SACON-F varied with different OA (C_{18}) contents. The SACON-F-15 organogel exhibited the optimal adhesive strength of 20.5 kPa, which was greater than that of SACON-F-10 (8.5 kPa) and SACON-F-25 (6.0 kPa). With the increased content of hydrophobic groups, the number of adhesion sites gradually increased to enhance the adhesive strength while massive C_{18} alkyl chains became entangled with one another and weakened the mechanical and adhesive behavior in the highly crosslinked state. The adhesive strengths of SAON-F, ACON-F, and SACON-F to glass, wood, metal, PE, PP, and polytetrafluoroethylene (PTFE) in air and underwater were quantitatively compared (Fig. S7a, b). The results revealed that the multiple noncovalent interactions significantly promoted underwater adhesion performance.

The underwater adhesion performance could be applied to various substrates. Fig. 4d and Fig. S7c–f illustrate the adhesion of SACON-F to PTFE, metal, and glass in air or underwater. Fig. 4e summarizes the specific adhesive strengths of SACON-F

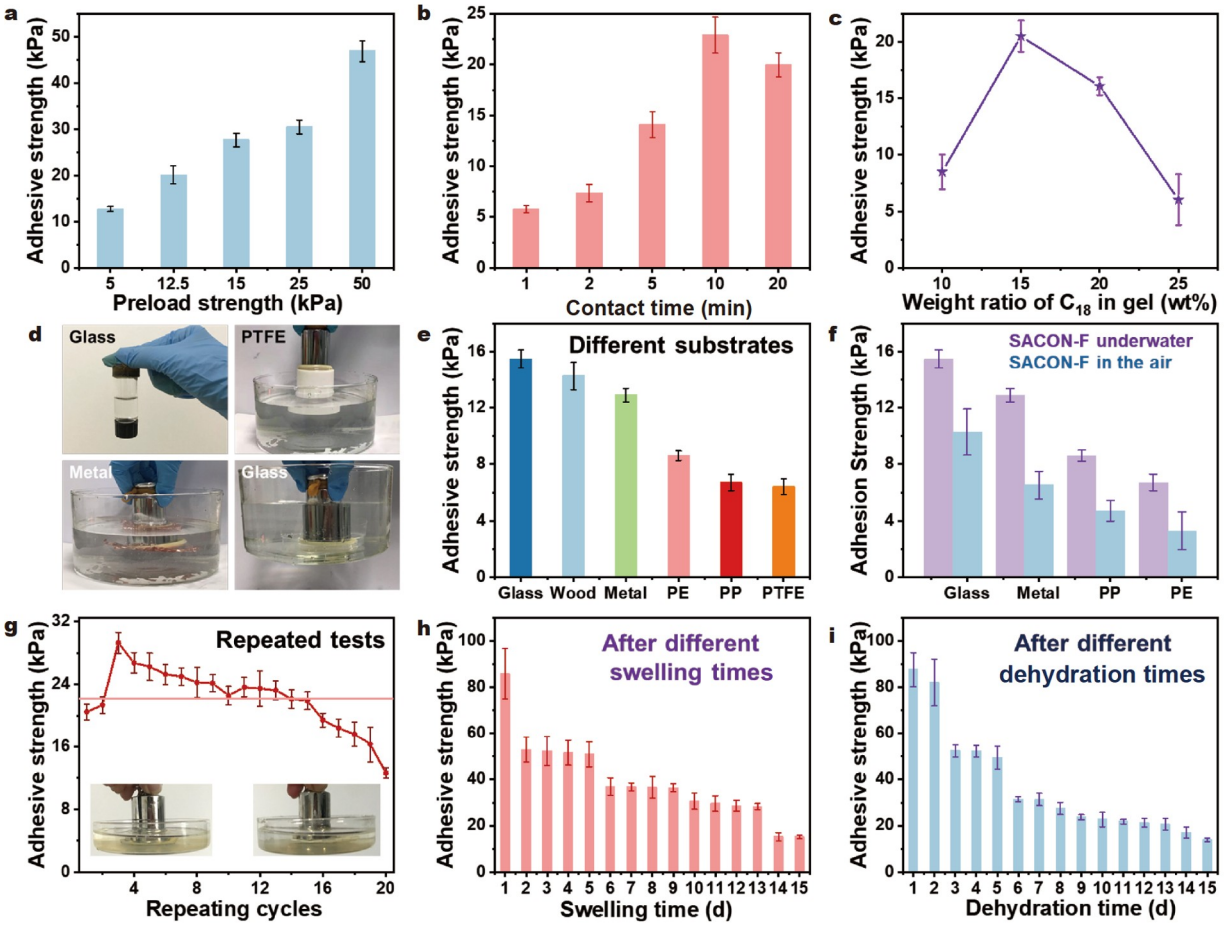

Figure 4 Underwater adhesion of organogels. (a, b) Adhesion strengths for different preload compression strengths (10 min, 5–50 kPa) and contact times (1–20 min, 25 kPa). (c) Adhesion strengths of SACON-F with different C_{18} fractions. (d) Photos of adhesive performance of SACON-F to glass in air, metal, PTFE, and glass underwater. (e) Adhesion strength of SACON-F to various substrates underwater. (f) Adhesion strength of SACON-F to different substrates in air and underwater. (g) Underwater adhesion strength after 20 consecutive attachment-detachment cycles. (h, i) Adhesive performance of SACON-F to glass during swelling and dehydration procedures.

to various substrates underwater, which are comparable to those in previous reports [34–36]. As shown in Fig. 4f, the adhesion strengths of SACON-F gel toward glass, metal, PE, and PP underwater (15.5, 12.9, 8.6, and 6.7 kPa) were significantly higher than those in the air (10.3, 6.5, 4.7, and 3.3 kPa, respectively) because the expulsion of water is an energy-favored process during the formation of the hydrophobic interface. Fig. 4g shows the evolution of adhesion strength under repeated adhesion-slip tests when SACON-F adhered to a glass substrate. The adhesion strength of SACON-F decreased gradually after long-term testing. After 20 cycles, SACON-F retained 62% of its original adhesion strength. In addition, SACON-F remained sticky during 15 days of storage in water (Fig. 4h) or 15 days of dehydration (Fig. 4i), thereby showing a comprehensible decline in adhesion strength of 15.3 and 14.0 kPa thereafter. The sustained adhesion after long-term storage in air and water is due to the self-hydrophobic effect from the hydrogel surfaces and the nonswellability of the organogels. The results emphasized the strong and long-lasting underwater adhesion ability of SACON-F that broadens its practical application to harsh aquatic environments.

Mechanical properties of SACNON-F

The two-step method for preparing the SACNON-F organogel is highly flexible and challenging. During the immersion process, the solvent exchange breaks the established hydrophobic association and induces the aggregation of hydrophobic monomers through simultaneous electrostatic interaction and metal-organic coordination, thus exerting a crucial effect on the mechanical performance of organogels. By modulating the immersion time in DMSO solutions, this study sets a solvent exchange time of 80 min to reach the optimal mechanical performance (Fig. S8a). Fig. 5a depicts the stress-strain curves of different organogels in air. The ultralong Ag NWs displayed apparent stretchability enhancement, as demonstrated in our previous research [10]. No distinct difference in stretchability was noted for the other three types of organogels. Meanwhile, the strength of the AON-F gel (80 kPa) was significantly reduced because of the absent metal-coordination interaction from catechol and Fe^{3+} [37]. With highly crosslinked covalent bonds and abundant reversible noncovalent interactions, as well as additional hydrophobic association, SACON-F achieved the optimal balance in stretchability (1567%) and fracture strength (302 kPa). Fig. 5b compares the tensile properties of the organogel in air and underwater. The strength (716 kPa) and strain at break (2191%) of SACON-F were more significantly enhanced in water than in air (302 kPa, 1567%). The fracture energy of SACON-F tested underwater was calculated to be 8.20×10^4 J m^{-2}. When stretched underwater, the hydrophobic segments in SACON-F could efficiently separate and dissipate energy while OA and SDS rapidly self-aggregated to enhance the hydrophobic association and thus enable impressive promotion in toughness and stretchability. SACON-F also showed outstanding compressive resilience at 20%, 25%, 30%, and 40% compressions (Fig. 5c). The addition of 0.1% Ag NWs significantly enhanced the compressive strength of the organogel in a similar way to the tensile property (Fig. 5d). With multiple reversible chemical and physical interactions in the polymer matrix, SACON-F could withstand 1044 tensile cycles at 268% strain (Fig. 5e) and 3981 cyclic compressions at 60% contraction (Fig. 5f) underwater with negligible mechanical degradation, thus showing excellent mechanical stability under deformation (Fig. S8b).

Electrical properties of SACON-F sensor underwater

The highly conductive and mechanically robust organogel with

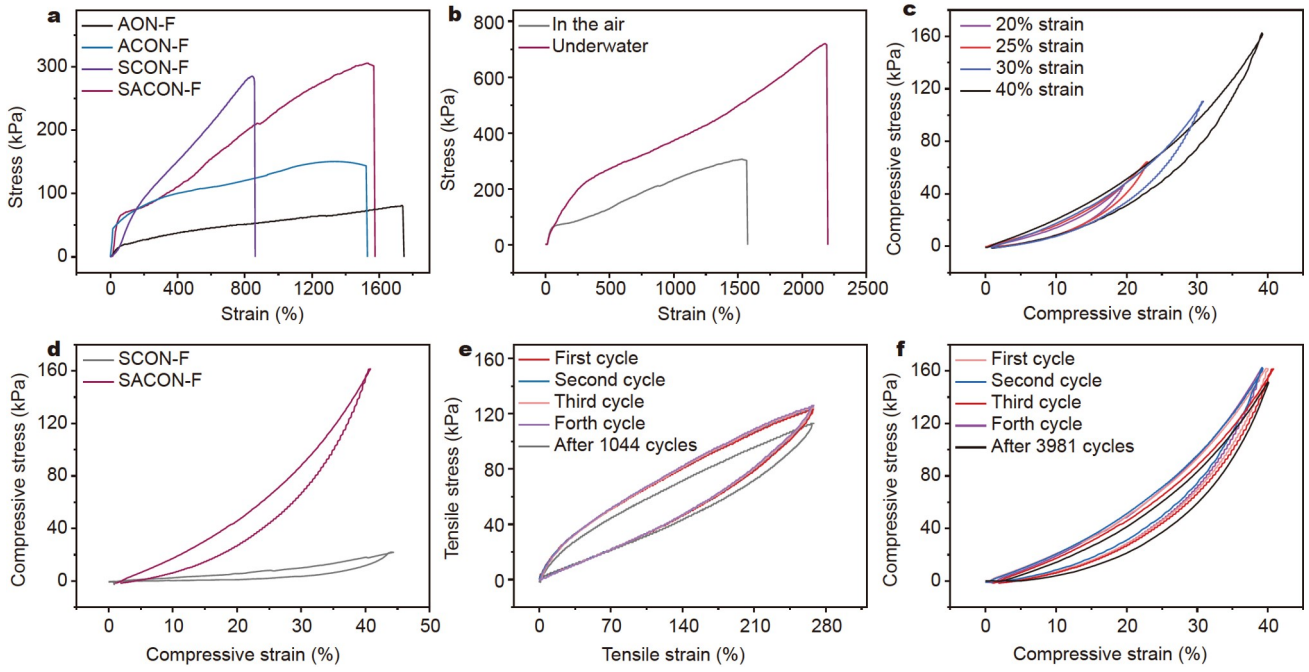

Figure 5 Mechanical performances of organogel sensors. (a) Strain-stress curves of AON-F, ACON-F, SCON-F, and SACON-F in air. (b) Mechanical performances of SACON-F in air and underwater. (c) Compression loading-unloading curves at 20%, 25%, 30%, and 40% strains underwater. (d) Compressive loading-unloading curves of SACON-F and SCON-F at 40% strain underwater. (e) Cyclic stretching-releasing curves at 268% strain underwater. (f) Compressive loading-unloading cycles at 60% contraction underwater.

antiswelling property enables the perception of different mechanical deformations. Fig. S9 demonstrates the electromechanical performance of the SACON-F sensor in air. SACON-F presented low hysteresis on mechanical deformation and displayed reliable, rapid, reproducible, and low limit perception to different ranges of strains at different frequencies. This result validated its high reliability in harsh environments. As presented in Fig. 6a, the sensitivity of the SACON-F sensor to mechanical deformation underwater revealed two characteristic stages as the applied tension increased. Specifically, a GF of 1.96 was achieved in the 0–70% strain range; this value applies to human motion detection (a maximum strain of 75% for human joint deformations [38]). The Ag NW nanofillers established a conductive network, and the Fe^{3+}-introduced electrostatic interaction provided sufficient electron transfer and ion conduction, simultaneously contributing to the enhanced sensitivity of the SACON-F sensor relative to the SCON-F (GF = 0.52) and SACON (GF = 1.01) counterparts. Moreover, the Ag NWs were anchored to the three-dimensional (3D) polymer framework and inhibited the slippage of the conductive network under large deformations. Together with the violent resistance variation from the tunneling effect [39,40], the SACON-F sensor revealed a higher GF of 13.52 when the strain exceeded 75%. The high sensitivity of the SACON-F sensor ensured the accurate recognition of mechanical deformations with different amplitudes.

Fig. 6b reveals that the SACON-F sensor displayed low hysteresis as the output electrical signal kept pace with the applied strain. This characteristic presents a foundation for the sensitive perception of real-time electromechanical responses. Fig. 6c describes the relative resistance change of the organogel sensor under different stretching degrees in air and underwater. When 100%, 400%, and 800% strains were applied to the organogel sensor at a frequency of 0.3 Hz, the relative resistance change gradually increased with the strains. The output electrical signals were uniform and stable, indicating that the sensor had high sensitivity and stability in the air and underwater. The gel sensor exhibited distinct relative resistance change underwater when subjected to the same strain. Such a result suggested that when the gel sensor is stretched underwater, more hydrophobic associations are exposed to weaken the metal-coordination interaction; consequently, the increased free carriers contribute to the enhanced conductivity, and the sensitivity of the organogel underwater is enhanced. The sensor underwater could also make a stable response to frequencies ranging from 0.06 to 0.22 Hz (Fig. 6d). This capability proves its accurate perception of quasistatic deformations and provides a necessary premise for human motion recognition in water. In addition, the gel sensor could respond quickly and sensitively to small strains underwater with a short response time of 158.1 ms (Fig. 6e), which is comparable to that obtained in the air (Fig. S9d). With an excellent antiswelling property and firm 3D polymer matrix, the SACON-F sensor demonstrated superior stability under deformation in water. As shown in Fig. 6f, the organogel sensor was subjected to repeated strain (71%) loading and releasing cycles at a frequency of 0.53 Hz. The corresponding resistance changes were the same during 1044 cycles, thereby confirming its long-term perception stability and high resistance to various harsh environments.

The excellent resilience of SACON-F also facilitates its application as a pressure sensor. Fig. 7a compares the sensitivities of SCON-F and SACON-F sensors underwater. The SACON-F pressure sensor displayed high sensitivity in a relatively wide monitoring range. The result revealed two stages of piezoresistive sensitivity: 5.22 kPa^{-1} in the low-pressure range (0–15 kPa) and 2.82 kPa^{-1} in the high-pressure range (15–35 kPa). The sensitive perception of the SACON-F sensor to pressure mainly depended on the uniformly distributed Ag NWs, whose connection, crimping, and entanglement dominated the evolution of the conductive network under different amplitude pressures. In comparison, the sensitivity of the

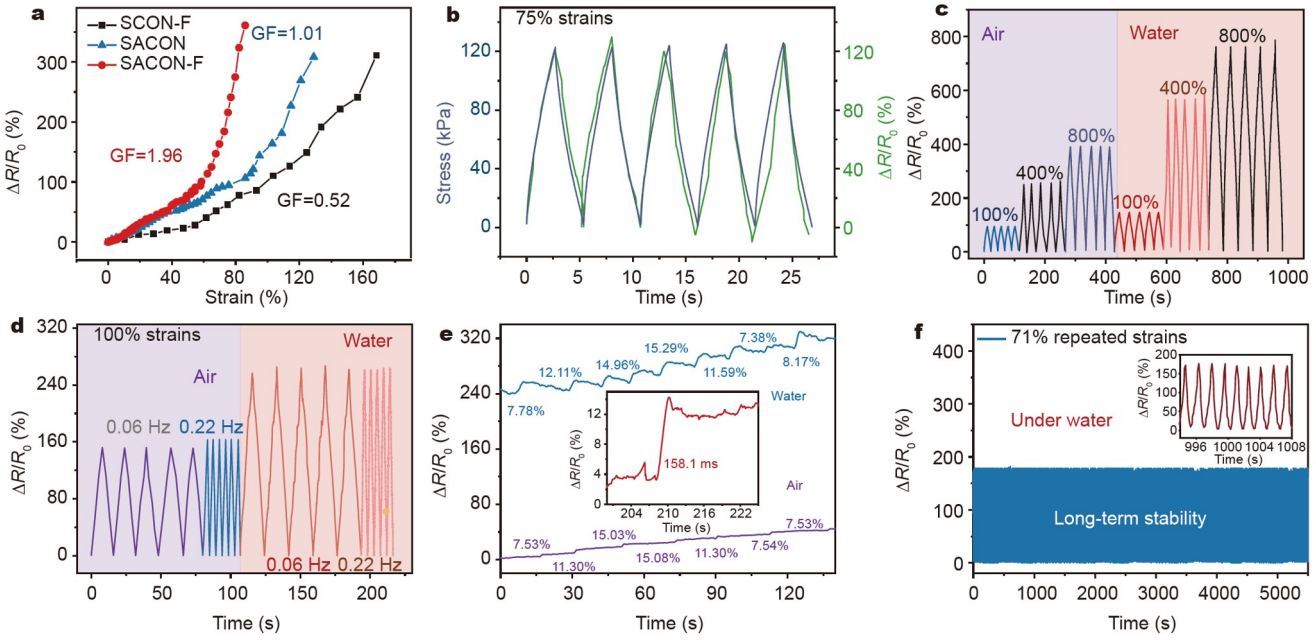

Figure 6 Electromechanical properties of organogel sensor underwater. (a) GF of SCON-F, SACON, and SACON-F sensors. (b) Hysteresis of SACON-F sensor. (c) Multicycle tests of sensors stretched to different strains (100%, 400%, and 800%). (d) Multicycle tests of relative resistance variation as a function of time upon stretching to 100% strain at different frequencies. (e) Response time under transient small strains. (f) Durability test of SACON-F sensor.

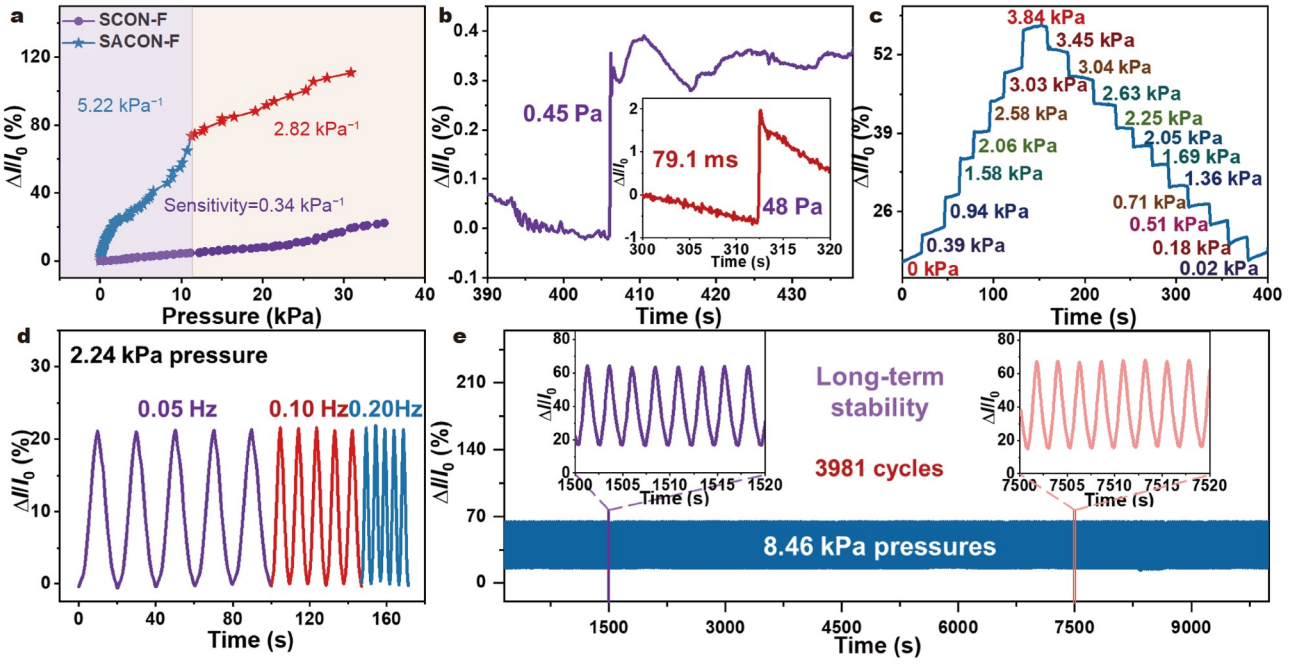

Figure 7 Electromechanical properties of organogel pressure sensor. (a) Sensitivity of SCON-F and SACON-F sensors. (b) Response time of SACON-F sensor underwater with instantaneous pressures. (c) Relative current changes of SACON-F sensor underwater with small pressures (less than 3.84 kPa). (d) Different current profiles of SACON-F sensor compressed underwater at different frequencies. (e) Long-term stability of SACON-F sensor underwater.

SCON-F sensor without Ag NWs showed a dramatic decline (0.34 kPa^{-1}) in the pressure range of 0–35 kPa. Fig. 7b demonstrates that the SACON-F pressure sensor presented a short response time of 79.1 ms underwater when an instantaneous pressure of 48 Pa was applied. It also exhibited an extraordinarily low detection limit of 0.45 Pa with 0.37% current variation. Fig. 7c shows the prompt and accurate response of the SACON-F pressure sensor to continuously varying subtle pressure levels. Subsequent experiments further indicated the high stability and high durability of the SACON-F pressure sensor. As displayed in Fig. 7d, 2.24 kPa was continuously applied to the SACON-F pressure sensor at different frequencies (0.05, 0.10, and 0.20 Hz). The current output waveforms were stable and consistent at various frequencies. The SACON-F sensor, in particular, demonstrated outstanding antifatigue features underwater with a highly reproducible current response (Fig. 7e) when subjected to persistent 3981 compression loading-releasing cyclic tests at 8.46 kPa.

Application of SACON-F sensor to human motion perception

The SACON-F sensor reveals high sensitivity, rapid response, low limit of detection, and ultrahigh stability in air and underwater. Such properties significantly broaden its application as a wearable electronic device. The underwater sensing performances of the gel sensor are presented as follows. Fig. 8a shows that the SACON-F sensor accurately recognized wrist joint movement patterns on the basis of the response signal amplitude and waveform. Moreover, Fig. 8b indicates that the organogel sensor could conformally attach to an index finger and accurately identify the bending process of fingers in different conditions. As the bending angle rose, the relative resistance changes increased accordingly. The repeated mechanical deformations led to consistent electrical characteristic peaks, indicating the high reliability of the sensor in human motion recognition. Fig. 8c, d, and Fig. S10d show the excellent response of the SACON-F sensor to facial expressions. The specific muscle movements in the corners of the mouth and eyes can be precisely monitored when opening or blinking at different paces, respectively. When the SACON-F sensor was installed on the throat, it could recognize the swallowing actions (Fig. 8e) and identify vocal cord vocalization (Fig. 8f). Each swallow action produced distinct and stable signal outputs, and the different words spoken corresponded to differentiable current responses with repetitive and consistent output waveforms (Fig. S10a–c). These properties make the sensor applicable to speech recognition and as a health monitoring tool for the disabled. The monitoring of pulse, breathing, and small vibration demonstrates the potential of the SACON-F sensor as a wearable device for real-time physiological health tracking (Fig. S11). The SACON-F sensor can also be assembled into a typical writing board for intelligent human-computer interaction. In Fig. 8h and Fig. S10e–g, the output signal could synchronically reflect alphabet writings of "I", "A", and "M" with different response current peak shapes in three consecutive cycles. Moreover, the writing board could distinguish the stroke patterns from different test takers (Fig. S12) and is thus applicable to handwriting identification. The writing board also operates reliably when writing underwater (Fig. 8i and Fig. S10h, i). This property thus expands the sensor's application to aquatic environments.

As the SACON-F sensor demonstrates extraordinary antiswelling properties and reliable mechanical and electrical performances in humidity, its application can be further extended to specific underwater situations. For noncontact underwater information transmission, the Morse code is identified as an effective approach to first aid and messaging. Fig. S13a presents the condition where deep-sea divers call for help when they are in danger. As manifested in Fig. 8g, through pressing the water surface with a tweezer in a short or long period, simulating the

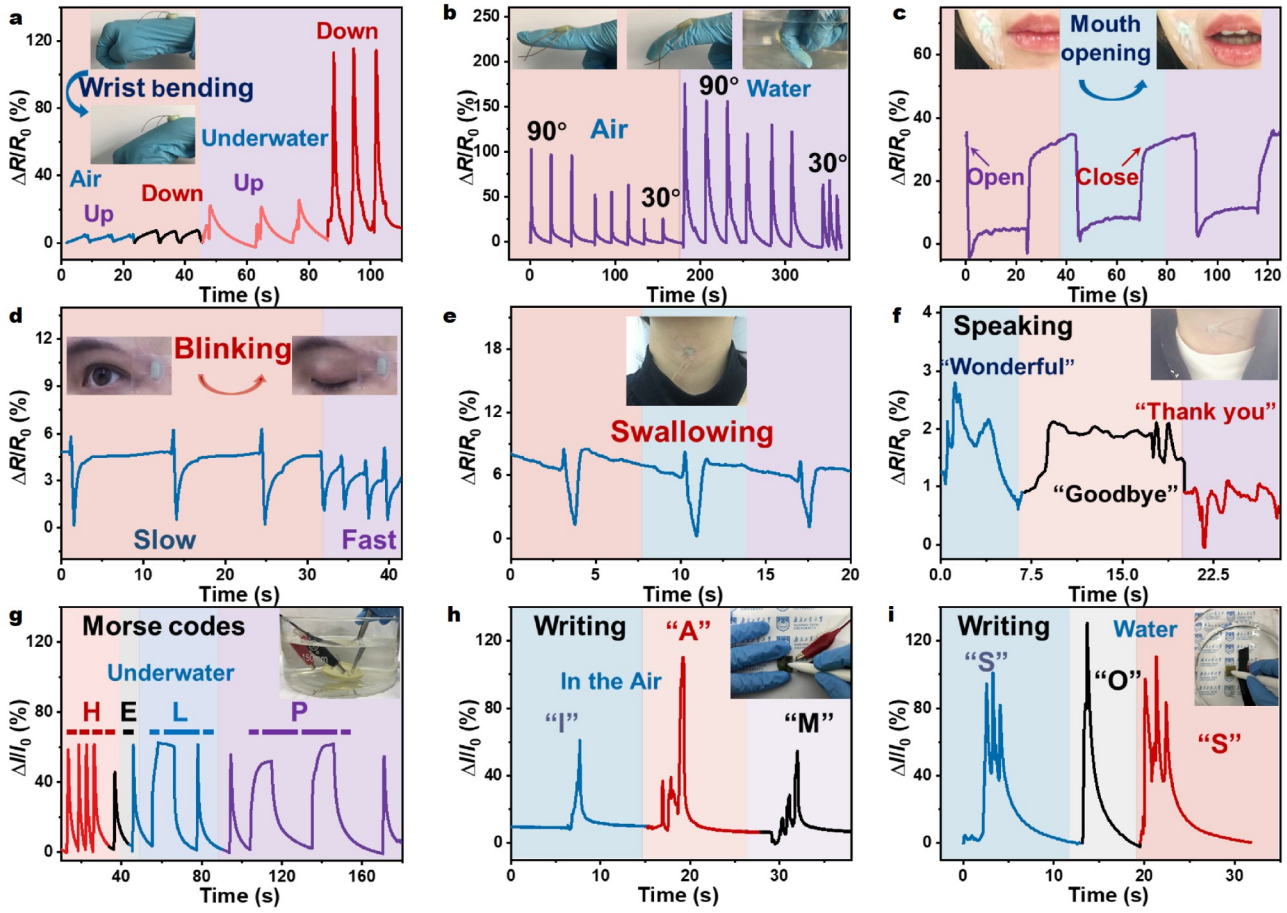

Figure 8 Sensing properties of SACON-F sensor. (a) Relative current variations of SACON-F sensor during wrist bending. (b) Electrical response with finger bending. (c, d) Piezoresistive responses to mouth opening and eye blinking. (e, f) Current response curves for swallowing and voice recognition. (g) SACON-F sensor communicates through Morse code underwater. (h, i) Relative current signals in the monitoring writing "I", "A", and "M" in air and "S" and "O" underwater.

Morse code arrangements of dots and dashes, the message of "HELP" could be captured in the form of electrical signal variations. Wireless communication could also be realized through the rhythmic tapping of water owing to the regular vibration conduction from water to the sensor surface. For instance, the message "HELP" and "DANGER" could be effectively transmitted by recording the peak numbers and durations per unit time (Fig. 9a, Fig. S14a). Fig. 9b shows that the water wave caused by slight blowing at the surface could be accurately monitored. Each disturbance of the water wave would produce a relative resistance change of 7%. The factors that induce water vibration were also evaluated herein to estimate the accuracy of the Morse code transmission. As demonstrated in Fig. 9c, when the finger is bent from 30° to 90° underwater gradually, the output current signal varies accordingly. The number of fingers touching the water surface also affects the vibration amplitude of the water surface, thus showing distinguishable current response output (Fig. S14e). By immersing objects of different weights in a water tank repeatedly, the high sensitivity of vibration perception was further emphasized (Fig. 9d and Fig. S14d). Even a tweezer of 6 g could induce apparent variation in relative current, thus suggesting a strict precalibration and firm encapsulation before practical applications. The noncontact Morse code information transmission could also be achieved in 3.5 wt% NaCl solutions (Fig. S14b, c), thus indicating potential applications in marine environments. The increase in resistance variation in the NaCl solution may be due to the changes in the conductivity of the solution.

Owing to their highly sensitive perception of water waves, the organogel sensor could distinguish gestures when hands touch the water surface, as described in Fig. 9e and Fig. S14g–i. The sensor demonstrated an evident relative resistance response when gestures of "Love", "OK", and "Good" were performed at the water surface. Apart from the above capabilities, the gel sensor could also sense ultrasound variation. In Fig. S14f, the SACON-F sensor (r = 22 mm) was put at the bottom of the ultrasonic machine, and different frequencies of ultrasound produced differential current signal outputs. The ultrasonic perception is applicable if the sensor were placed underwater. Fig. 9f presents stable and reproducible current signal output in detecting ultrasound vibrations underwater. Fig. S13b comprehensively compares the SACON-F sensor with other gel-based sensors employed under aquatic conditions. The results demonstrate the sensor's enhanced performance for flexible wearable electronics in underwater motion detection, underwater robot motion recognition, and other various harsh environments.

CONCLUSION

In summary, a hydrophobic organogel (SACON-F) based on

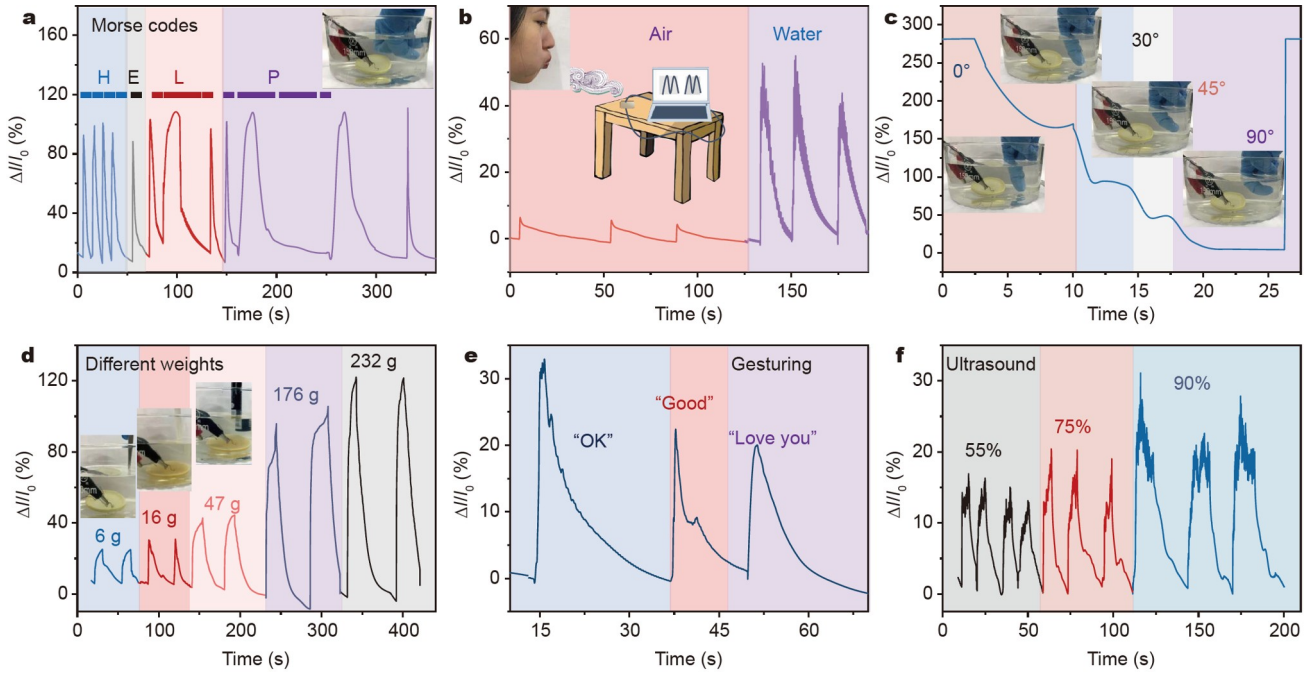

Figure 9 Underwater sensing properties of SACON-F sensor. (a) Piezoresistive response of "HELP" when touching the water surface to transmit the Morse codes remotely. (b) The current response of slight blowing on the sensor surface in air and underwater. (c) Current response curves for remote detection of finger bending at different angles. (d) Recognition of immersed objects (scissors, pen, glass mold, and beaker) in water with different weights. (e) Relative current signals in monitoring gestures "OK", "GOOD", and "LOVE YOU" underwater. (f) Relative current signals in detecting ultrasound vibrations underwater.

micelle aggregation and metal ion coordination was prepared for high-sensitivity underwater sensors. The organogel possessed excellent antiswelling and antidehydration properties. The abundant dynamic noncovalent interactions also endowed the organogel with excellent hydrophobicity and superior underwater adhesion for applications in aquatic environments. Moreover, the fabricated organogel sensor exhibited highly sensitive (GF = 1.96) and reproducible responses to different forms of deformations with fast response (~79.1 ms) in air and underwater. Hence, this sensor shows promise in diverse mechanical perceptions in various harsh environments. The prepared sensor was applied to a range of force detections in contact and contactless modes. The results reveal its great promise in a wide range of remote underwater signal transmission applications.

Received 17 December 2021; accepted 21 February 2022; published online 1 April 2022

1 Jung H, Kim MK, Lee JY, *et al.* Adhesive hydrogel patch with enhanced strength and adhesiveness to skin for transdermal drug delivery. Adv Funct Mater, 2020, 30: 2004407
2 Ge G, Huang W, Shao J, Dong X. Recent progress of flexible and wearable strain sensors for human motion monitoring. J Semicond, 2018, 39: 011102
3 Ge G, Yuan W, Zhao W, *et al.* Highly stretchable and autonomously healable epidermal sensor based on multi-functional hydrogel frameworks. J Mater Chem A, 2019, 7: 5949–5956
4 Cui C, Wu T, Gao F, *et al.* An autolytic high strength instant adhesive hydrogel for emergency self-rescue. Adv Funct Mater, 2018, 28: 1804925
5 Zhang K, Zhao Z, Huang J, *et al.* Self-recoverable semi-crystalline hydrogels with thermomechanics and shape memory performance. Sci China Mater, 2019, 62: 586–596
6 Pan Z, Wang ZY, Wang MH, *et al.* Adhesive aero-hydrogel hybrid conductor assembled from silver nanowire architectures. Sci China Mater, 2021, 64: 2868–2876
7 Yuan W, Qu X, Lu Y, *et al.* MXene-composited highly stretchable, sensitive and durable hydrogel for flexible strain sensors. Chin Chem Lett, 2020, 32: 2021–2026
8 Ge G, Lu Y, Qu X, *et al.* Muscle-inspired self-healing hydrogels for strain and temperature sensor. ACS Nano, 2020, 14: 218–228
9 Chen D, Pei Q. Electronic muscles and skins: A review of soft sensors and actuators. Chem Rev, 2017, 117: 11239–11268
10 Zhao W, Qu X, Xu Q, *et al.* Ultrastretchable, self-healable, and wearable epidermal sensors based on ultralong Ag nanowires composited binary-networked hydrogels. Adv Electron Mater, 2020, 6: 2000267
11 Cai Y, Shen J, Ge G, *et al.* Stretchable $Ti_3C_2T_x$ MXene/carbon nanotube composite based strain sensor with ultrahigh sensitivity and tunable sensing range. ACS Nano, 2018, 12: 56–62
12 Lu Y, Qu X, Zhao W, *et al.* Highly stretchable, elastic, and sensitive MXene-based hydrogel for flexible strain and pressure sensors. Research, 2020, 2020: 1–13
13 Li J, Celiz AD, Yang J, *et al.* Tough adhesives for diverse wet surfaces. Science, 2017, 357: 378–381
14 Liu X, Zhang Q, Jia F, *et al.* Underwater flexible mechanoreceptors constructed by anti-swelling self-healable hydrogel. Sci China Mater, 2021, 64: 3069–3078
15 Zhao T, Wang G, Hao D, *et al.* Macroscopic layered organogel-hydrogel hybrids with controllable wetting and swelling performance. Adv Funct Mater, 2018, 28: 1800793
16 Liu X, Zhang Q, Duan L, *et al.* Tough adhesion of nucleobase-tackifed gels in diverse solvents. Adv Funct Mater, 2019, 29: 1900450
17 Zhong C, Gurry T, Cheng AA, *et al.* Strong underwater adhesives made by self-assembling multi-protein nanofibres. Nat Nanotech, 2014, 9: 858–866
18 Baik S, Lee HJ, Kim DW, *et al.* Bioinspired adhesive architectures: From skin patch to integrated bioelectronics. Adv Mater, 2019, 31: 1803309
19 Wei W, Yu J, Broomell C, *et al.* Hydrophobic enhancement of dopa-mediated adhesion in a mussel foot protein. J Am Chem Soc, 2012, 135: 377–383
20 Xu L, Gao S, Guo Q, *et al.* A solvent-exchange strategy to regulate

noncovalent interactions for strong and antiswelling hydrogels. Adv Mater, 2020, 32: 2004579
21 Ji S, Wan C, Wang T, *et al.* Water-resistant conformal hybrid electrodes for aquatic endurable electrocardiographic monitoring. Adv Mater, 2020, 32: 2001496
22 Fan X, Fang Y, Zhou W, *et al.* Mussel foot protein inspired tough tissue-selective underwater adhesive hydrogel. Mater Horiz, 2021, 8: 997–1007
23 Zhang W, Wang R, Sun ZM, *et al.* Catechol-functionalized hydrogels: Biomimetic design, adhesion mechanism, and biomedical applications. Chem Soc Rev, 2020, 49: 433–464
24 Qu X, Wang S, Zhao Y, *et al.* Skin-inspired highly stretchable, tough and adhesive hydrogels for tissue-attached sensor. Chem Eng J, 2021, 425: 131523
25 Guo Q, Chen J, Wang J, *et al.* Recent progress in synthesis and application of mussel-inspired adhesives. Nanoscale, 2020, 12: 1307–1324
26 Han L, Wang M, Prieto-López LO, *et al.* Self-hydrophobization in a dynamic hydrogel for creating nonspecific repeatable underwater adhesion. Adv Funct Mater, 2019, 30: 1907064
27 Su X, Luo Y, Tian Z, *et al.* Ctenophore-inspired hydrogels for efficient and repeatable underwater specific adhesion to biotic surfaces. Mater Horiz, 2020, 7: 2651–2661
28 Gan D, Xing W, Jiang L, *et al.* Plant-inspired adhesive and tough hydrogel based on Ag-lignin nanoparticles-triggered dynamic redox catechol chemistry. Nat Commun, 2019, 10: 1487
29 Deng Z, Yu R, Guo B. Stimuli-responsive conductive hydrogels: Design, properties, and applications. Mater Chem Front, 2021, 5: 2092–2123
30 Deng Z, Wang H, Ma PX, *et al.* Self-healing conductive hydrogels: Preparation, properties and applications. Nanoscale, 2020, 12: 1224–1246
31 Lin L, Liu M, Chen L, *et al.* Bio-inspired hierarchical macromolecule-nanoclay hydrogels for robust underwater superoleophobicity. Adv Mater, 2010, 22: 4826–4830
32 de Oliveira TE, Mukherji D, Kremer K, *et al.* Effects of stereochemistry and copolymerization on the LCST of PNIPAm. J Chem Phys, 2017, 146: 034904
33 Gao Y, Chen J, Han X, *et al.* A universal strategy for tough adhesion of wet soft material. Adv Funct Mater, 2020, 30: 2003207
34 Cui C, Fan C, Wu Y, *et al.* Water-triggered hyperbranched polymer universal adhesives: From strong underwater adhesion to rapid sealing hemostasis. Adv Mater, 2019, 31: 1905761
35 Zhao Y, Wu Y, Wang L, *et al.* Bio-inspired reversible underwater adhesive. Nat Commun, 2017, 8: 2218
36 Wang P, Pu Y, Ren Y, *et al.* Bio-inspired hydrogel-based bandage with robust adhesive and antibacterial abilities for skin closure. Sci China Mater, 2022, 65: 246–254
37 Zeng H, Hwang DS, Israelachvili JN, *et al.* Strong reversible Fe^{3+}-mediated bridging between dopa-containing protein films in water. Proc Natl Acad Sci USA, 2010, 107: 12850–12853
38 Gu Z, Xu Y, Chen L, *et al.* Macroporous conductive hydrogels with fatigue resistance as strain sensor for human motion monitoring. Macromol Mater Eng, 2018, 303: 1800339
39 Shi Y, Xiong D, Liu Y, *et al.* Swelling, mechanical and friction properties of PVA/PVP hydrogels after swelling in osmotic pressure solution. Mater Sci Eng-C, 2016, 65: 172–180
40 Cai Y, Shen J, Dai Z, *et al.* Extraordinarily stretchable all-carbon collaborative nanoarchitectures for epidermal sensors. Adv Mater, 2017, 29: 1606411

Acknowledgements This work was supported by the Natural Science Foundation of Jiangsu Province (BK20190688), the Natural Science Foundation of Jiangsu Higher Education Institutions (21KJB430039), and Taishan Scholar Construction Special Fund of Shandong Province.

Author contributions Wang Q and Zhao W designed and conducted the experiments. Gan D, Qu X, Liu J, and Liu Y supervised the theoretical and experimental work. Zhao W wrote and revised the manuscript with support from Dong X, Sun C, and Wang W. All authors contributed to the data analysis, discussed the results, and commented on the manuscript.

Conflict of interest The authors declare that they have no conflict of interest.

Supplementary information Supporting data are available in the online version of the paper.

Wen Zhao received her BSc and Master's degrees in optoelectronics information science and engineering from Nanjing Tech University and is currently a PhD candidate at the City University of Hong Kong. Her research mainly focuses on flexible hydrogel electronics and biomechanical devices for health monitoring.

Chencheng Sun is currently working as an assistant professor at Changshu Institute of Technology. He obtained his PhD degree from Nanjing Tech University in 2016. His research mainly focuses on the design and fabrication of energy storage materials and devices, such as nanocarbon materials, flexible supercapacitors and lithium-ion batteries.

Qian Wang received her PhD degree from the University of Chinese Academy of Sciences in 2015. Then, she continued postdoctoral research at Shanghai Institute of Microsystem and Information Technology, Chinese Academy of Sciences for three years. Her current research interest focuses on the design and preparation of nanomaterials for flexible electronics.

Xiaochen Dong earned his PhD degree from Zhejiang University in 2007. Then he did postdoctoral research at Nanyang Technological University in Singapore. In 2012, he joined Nanjing Tech University as a full professor. He was supported by the National Science Fund for Distinguished Young Scholars in 2015. His research interests are nanomaterials for bio-optoelectronics, energy conversion and storage.

一种生物启发的疏水有机凝胶在高灵敏力学感应方面的应用

赵雯[1,4], 甘鼎立[1], 曲心宇[1], 刘静莹[1], 刘云龙[2], 王倩[1*], 王文军[2], 孙陈诚[3*], 董晓臣[1*]

摘要 柔性电子设备, 特别是在潮湿环境中仍具备机械力感知功能的传感设备, 是目前智能传感领域的新前沿. 受海洋生物在水下环境适应性强特点的启发, 我们制备了一种具有强水下粘附性、良好疏水性、抗溶胀性和水下力学检测的高灵敏有机凝胶传感器. 凝胶内部大量可逆非共价键的协同作用确保了其在水下对多种基底均具有粘附能力; 同时, 通过调节化学组分和内部相互作用, 使得该凝胶具备疏水性(接触角111.8°)与抗溶胀性(15天平衡溶胀率为−31%), 制备的柔性应变传感器灵敏度高(GF因子为1.96)、响应迅速(响应时间79.1 ms)、检测限低(0.45 Pa)、循环稳定性优异(可承受不少于1044个拉伸循环以及3981个压缩循环加载), 其在空气中和水中均可实现对复杂人体运动的精确感知, 在海洋勘探领域具有广阔的应用前景.

